



Interaction-energy landscapes of kagome and honeycomb lattices of dipole-coupled magnetic nanoparticles

David Gallina * and G. M. Pastor *Institut für Theoretische Physik, Universität Kassel, Heinrich-Plett-Straße 40, 34132 Kassel, Germany*

(Received 8 October 2023; accepted 28 November 2023; published 11 December 2023)

The collective magnetic behaviors of dipole-coupled magnetic nanoparticles organized in periodic two-dimensional kagome and honeycomb lattices are investigated theoretically. The extended nanostructures are modeled by considering finite unit cells containing nanoparticles with periodic boundary conditions. The energy landscapes (ELs) of the ensembles are systematically explored as a function of the orientation of all the NP moments by calculating the local minima and first-order saddle points connecting them. The low-lying magnetic orders and elementary reorientation transitions are identified. The thus obtained kinetic networks and disconnectivity graphs of the ELs reveal profound differences in the topology of the networks of stationary states. One observes that the honeycomb nanostructures are typically good structure seekers with starlike kinetic networks and palm-tree-like disconnectivity graphs. They have a continuously degenerate ground state, which is the center of the network and directly connected to all excited metastable states. In contrast, kagome nanostructures show a particular form of bad structure seeker, which is known as the latticelike stationary-point network. In this case, from a local perspective, the degree distribution among the LM is extremely homogeneous, with no centers or hubs through which relaxation can be funneled. Furthermore, from an energy perspective, no hierarchy among the low-energy metastable states can be identified.

DOI: [10.1103/PhysRevB.108.224412](https://doi.org/10.1103/PhysRevB.108.224412)

I. INTRODUCTION

Recent progress in the synthesis, self-assembly, and structuring of magnetic nanoparticles (NPs) has made it possible to fabricate artificial two-dimensional (2D) materials consisting of size-controlled and geometrically organized nanoscale magnets [1–5]. These systems constitute a highly dynamic and demanding current field of research, which addresses a number of challenging questions not only from a fundamental perspective but also in view of practical applications. Indeed the combination of finite-size effects, reduced dimensionality, and frustrating interactions gives rise to new magnetic phenomena that hold significant importance for potential uses in spintronics, memory devices, and high-density data storage [6–9].

The magnetic properties of NP ensembles are conditioned by a number of factors, among which the size and composition of the NPs, the type and strength of their interactions, and their geometrical arrangement deserve special attention. Pioneering studies into nanoscale magnetism, which primarily aimed to understand the impact of size, structure, and composition of individual nanoscale magnets, have revealed several fascinating effects, such as the remarkable enhancements of the spin moments, orbital moments, and magnetocrystalline anisotropy in small transition-metal clusters, or the onset of magnetism in clusters of nonmagnetic solids [10–19]. Furthermore, in more recent years, there has been a growing interest in understanding the collective magnetic response of extended

nanostructures composed of NP ensembles [4,5,20–25]. From this perspective, two qualitatively distinct regimes can be identified, depending on the relative strength of single-particle local energies and interparticle couplings. In situations where the interactions are relatively weak, the magnetic properties of the ensembles are primarily governed by individual particle attributes such as magnetization and anisotropy. The dynamics of such a system largely consists of local reorientations of the magnetic moments of individual NPs. As a result, the specific arrangement of the NPs is rather unimportant. A considerably more intricate and demanding scenario emerges when the interactions between particles are substantial, for example, in nanostructures composed of closely packed, highly symmetric NPs having weak magnetocrystalline anisotropies. In this case, a change in the orientation of the magnetic moment of one NP unavoidably leads to modifications in the magnetic order of adjacent particles. The cooperative magnetic behavior of the entire system becomes evident. Even the most basic transitions between two nearby metastable configurations involve reorientations of many NPs moments [26–28]. Clearly, the geometrical arrangement of the particles in the nanostructure and its point-group and translational symmetries, or the absence thereof, become crucial. The physical consequences are expected to be particularly important for the dipole-coupled NP ensembles investigated in this paper, since these interactions are both long range and frustrating [21,25–30].

Earlier studies of the magnetic properties of 2D NP ensembles have revealed a diverse range of captivating physical phenomena including phase transitions, continuous ground-state degeneracies, and order-by-disorder effects

*gallina@uni-kassel.de

[20,21,29–34]. In addition, remarkable nonequilibrium phenomena have been identified such as slowing down, ergodicity breaking, memory effects, and aging [35–38]. Recently, the behavior of 2D ensembles of magnetic NPs has been investigated by considering all possible periodic Bravais-lattice geometries, namely, square, triangular, rectangular, rhombic, and oblique lattices [39]. This study has revealed a remarkable dependence of the interaction-energy landscapes on the structural arrangement of the NPs. It has also established interesting correlations between the different collective magnetic behaviors and the specific point-group symmetries. Nevertheless, the properties of more complex nanostructures, which cannot be reduced to simple Bravais lattices, remain largely unexplored [40,41]. Two NP arrangements of considerable theoretical and practical interest are the honeycomb and kagome lattices. From the point of view of translations, both structures share the symmetry of the triangular Bravais lattice. However, the bases are different: dimers or hexagons for the honeycomb lattice and triangles for the kagome lattice. These differences profoundly affect the local point-group symmetries and are expected to have a significant influence on the physical behavior [31,40–42]. It is the goal of the present work to investigate the collective magnetic properties of honeycomb and kagome ensembles of magnetic NPs by characterizing their ELs and by correlating their magnetic behaviors to the underlying point-group and translational symmetries. Apart from the fundamental theoretical significance of establishing links between structural NP organization and collective magnetic behavior, this study is expected to serve as a benchmark for assessing the physics in more realistic scenarios including, for example, structural disorder, particle-size distributions, or magnetic anisotropies.

The remainder of the paper is organized as follows. In Sec. II, the model is introduced and the various methods employed for the characterization of the ELs are presented. The results for honeycomb and kagome lattices are presented and discussed in Sec. III, by contrasting in particular their metastable magnetic configurations, kinetic networks, and disconnectivity graphs. The paper is closed in Sec. IV with a summary of the main conclusions and by pointing out some relevant extensions and implications of the present study.

II. THEORETICAL MODEL AND METHODS

The interaction energy of a system of classical dipole-coupled magnetic moments $\vec{\mu}_k$, which are located at the lattice positions \vec{r}_k , is given by

$$E = \frac{\mu_0}{8\pi} \sum_{k \neq l} \left[\frac{\vec{\mu}_k \cdot \vec{\mu}_l}{r_{kl}^3} - 3 \frac{(\vec{\mu}_k \cdot \vec{r}_{kl})(\vec{\mu}_l \cdot \vec{r}_{kl})}{r_{kl}^5} \right], \quad (1)$$

where the vector $\vec{r}_{kl} = \vec{r}_k - \vec{r}_l$ connects lattice sites k and l , r_{kl} is the corresponding Euclidean distance, and μ_0 is the vacuum permeability. In the present model the magnetic moments $\vec{\mu}_k$ have a fixed modulus. Their orientations are defined by the polar and azimuthal angles θ_k and φ_k . Extended nanostructures are described by considering a finite number N of nanoparticles in a unit cell with periodic boundary conditions.

A. Stationary points

The static and dynamic properties of a magnetic NP ensemble are governed by its underlying EL, which in the present case depends on the $2N$ degrees of freedom $\{\theta_k, \varphi_k \mid k = 1, \dots, N\}$ defining the orientation of the magnetic moments $\vec{\mu}_k$ in space. A most practical way to simplify this intricate and complex multivariable function is to discretize it into its stationary states, specifically, its local minima (LM) and first-order saddle points or transition states (TSs) [43,44]. These stationary points form an interconnected network that allows us to describe the long-time stochastic dynamics of the system by focusing on the rare and mostly collective processes while disregarding the short-time fluctuations of the magnetic moments around the local minima.

The LM and TSs are identified using the following procedure, which has been adapted from the methodology outlined in Ref. [45]. At first, an initial set of metastable states is created by performing a number of local optimizations of the interaction energy starting from random configurations [46]. Then, the following steps are executed sequentially.

(i) Select a local minimum from the set of stationary states that has not yet been used for identifying new stationary states.

(ii) Perform an eigenvector-following search starting along a specific eigenvector of the Hessian $\hat{\mathbf{H}}$ at this LM [43,47]. Typically, the eigenvectors associated with the lowest eigenvalues of $\hat{\mathbf{H}}$ are chosen, since these directions yield the smallest energy increase as one moves away from the LM.

(iii) Upon finding a TS, the two adjacent LM are determined by stepping away from the TS in the directions that are parallel and antiparallel to the sole unstable mode and, starting from there, by performing the corresponding Limited-memory Broyden-Fletcher-Goldfarb-Shanno algorithm (L-BFGS) minimizations.

(iv) Most often, one of the two LM identified in the previous step coincides with the initial LM. In this case the other LM and TSs are added to the set of stationary states. If not, the TSs and LM are disregarded.

(v) The algorithm advances by selecting a different eigenvector and repeating steps (ii)–(iv). Once a certain number of eigenvectors ν_e have been tried (in this work $\nu_e = 10$), the algorithm goes back to step (i) and a new LM is taken into consideration.

The algorithm terminates after all LM in the database have been used as initial states. The result is the aimed set of stationary points of the EL.

B. Kinetic networks

The set of all LM and TSs of an energy landscape constitutes a connected network, often referred to as the kinetic network (KN) of the system. It can be visualized by an undirected graph, where the nodes represent the LM and the edges the elementary transitions that connect two LM through a first-order TS. Several properties can be calculated in order to characterize the various kinetic networks, thus allowing one to compare the topology of the ELs in different physical situations. The *degree* $n(i)$ of node i is the number of nodes which can be reached from the node i by a single elementary transition. It is given by the number of edges or TSs connecting node i with any other node. As the size of these networks

may vary strongly, it is sound to introduce the *degree density*

$$\rho(i) = \frac{n(i)}{N_{\text{LM}} - 1}, \quad (2)$$

where N_{LM} is the total number of LM in the network. Nodes with large values of $\rho(i)$ are known as *hubs*. Very often they play a central role in the dynamics of complex systems, since the relaxation across significant portions of the EL can be funneled through them.

Another important network property is the *distance* d_{ij} between nodes i and j , which is defined as the smallest number of steps or edges required to establish a connection between them. The *average path distance* $\langle d \rangle$ calculated over all pairs of nodes provides a measure of the overall extent of a network. Complementary information from a local perspective is obtained by assessing the level of clustering within the network. An established measure of this is the *transitivity*

$$C = \frac{3 \times \text{number of triangles}}{\text{number of triads}}, \quad (3)$$

which represents the probability that in a triad of nodes ($i \neq j \neq k$), where i is connected to j and j is connected to k , also i and k are directly connected [48].

C. Disconnectivity graphs

The concept of a disconnectivity graph (DG), introduced Becker and Karplus, offers a valuable means to visualize and analyze complex ELs by focusing on the energies of the LM and the energy barriers that separate them [49]. Several examples of DGs are shown in Sec. III. The physical interpretation of these graphs becomes clear once the procedure employed to generate them is outlined (see also Refs. [43,49]). For a given energy E , the LM with energies lower than E form distinct sets termed superbasins. Within each of these superbasins, the minimum energy path (MEP) between any pair of LM never exceeds the energy E . Typically, one starts the procedure by selecting a value E that is slightly above the energy of the global minimum. In the absence of degeneracies, only one superbasin containing the global minimum is accessible at this energy. But if the ground state is n -fold degenerate, one starts from n separate superbasins. As the energy E is progressively raised, additional LM are found whose energy is lower than E . However, note that these new LM cannot be linked with each other or to the lower-lying ones without exceeding E as long as E remains lower than the separating energy barriers. Consequently, the number of superbasins tends to increase initially. Nevertheless, at some point, for even larger E , the superbasins start to merge with each other, since the separating energy barriers along the connecting MEP can be overcome. Ultimately, at considerably higher energies, just a single superbasin remains, containing all the LM of the system, provided that the energy barriers are finite.

In practice, the DGs are constructed by applying the previously outlined analysis at predefined evenly spaced values of E , which are indicated on the y axis. For each energy E , a superbasin is depicted as a vertical segment. Two segments are connected with each other, if they share at least one local minimum. Since the positions of the superbasins along the horizontal x axis have no physical meaning and are *a priori*

arbitrary, they are chosen in order to optimize the readability of the graph. Usually, superbasins separated by smaller energy barriers are closer than those separated by larger barriers. As a result, a treelike graph is formed, where the end point of each branch reflects the energy of the corresponding local minimum and the junction of two branches indicates the energy barrier separating them. In the following section representative examples of DGs are discussed in some detail.

III. RESULTS

The primary purpose of this section is to identify the characteristic magnetic properties of dipole-coupled magnetic NPs forming perfectly periodic kagome or honeycomb lattices by analyzing the corresponding interaction-energy landscapes. The thus obtained insights are particularly important concerning the relation between magnetic behavior and lattice symmetry from a fundamental point of view. Moreover, they are very useful as a reference for understanding the consequences of structural disorder, which is inherent to any realistic experimental sample [50].

The extended nanostructures are modeled with finite unit cells having N magnetic NPs and periodic boundary conditions. To simplify comparisons between different ensembles, the energies are measured in units of the dipole-interaction energy ε_{DD} of a pair of parallel nearest-neighbor (NN) magnetic moments which are perpendicular to the vector connecting them. This is given by

$$\varepsilon_{DD} = \frac{\mu_0 \mu^2}{8\pi \lambda^3}, \quad (4)$$

where λ is the nearest-neighbor distance. For instance, to give an order of magnitude, in a system composed of ferromagnetic particles with a diameter $r = 3$ nm and a nearest-neighbor distance $\lambda = 5$ nm, we have $\varepsilon_{DD} = 1.4$ meV.

A. Honeycomb lattice

The 2D honeycomb lattice is defined by a triangular Bravais lattice with primitive translation vectors

$$\vec{e}_1 = \sqrt{3}\lambda(0, 1) \quad \text{and} \quad \vec{e}_2 = \frac{\sqrt{3}}{2}\lambda(\sqrt{3}, 1), \quad (5)$$

with a basis consisting of two sites A and B whose coordinates are

$$\vec{e}_A = (0, 0) \quad \text{and} \quad \vec{e}_B = \frac{\lambda}{2}(1, -\sqrt{3}), \quad (6)$$

where λ is the nearest-neighbor distance. This lattice has a D_3 point-group symmetry with respect to each lattice site, which consists of 6 different symmetry operations: the identity E , the $2\pi/3$ rotations C_3 and C_3^2 around the axis perpendicular to the lattice plane, and the three reflections across the planes defined by the NN bonds and the lattice normal. In addition, the honeycomb lattice has a D_6 point-group symmetry with respect to the center of each hexagon. This involves 12 different symmetry operations: the identity E ; the $\pi/3$ rotations C_6 , C_6^2 , C_6^3 , C_6^4 , and C_6^5 around the axis perpendicular to the lattice plane; and the six reflections across the planes perpendicular to the lattice and passing either through the middle of the NN bonds forming the hexagon or through two opposite corners

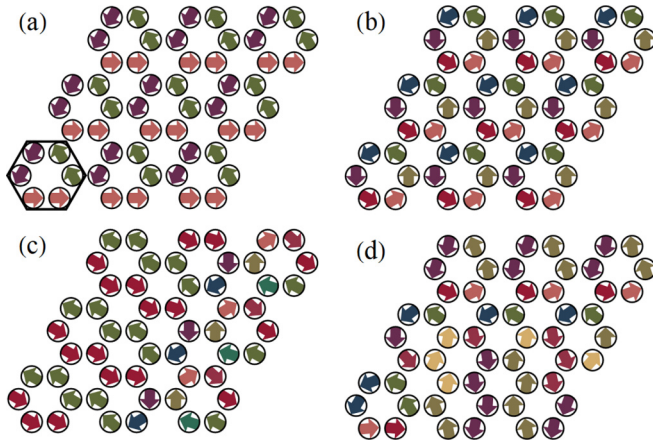


FIG. 1. Low-lying metastable magnetic configurations of a periodic honeycomb lattice with $N = 54$ dipole-coupled NPs in the unit cell. The circles indicate the position of the particles and the arrows the orientations of the magnetic moments within the xy plane. In panels (a) and (b), examples of the continuously degenerate ground state are shown with microvortex angles (a) $\eta_{MV} = 0$ and (b) $\eta_{MV} = \pi/2$. The magnetic configurations of the first- and second-excited states are shown in panels (c) and (d), respectively.

of the hexagon. Finally, as any monolayer planar structure, the lattice is invariant upon reflection across the lattice plane.

Figure 1 shows representative magnetic configurations of the degenerate ground states and of the first- and second-excited states of the honeycomb lattice as obtained with $N = 54$ MNPs in the unit cell. In all these configurations the magnetic moments are strictly parallel to the lattice xy plane. In fact, our energy minimizations starting from random spin orientations always yield local minima with only in-plane moments. The same holds for the obtained first-order saddle points and the associated minimum energy paths. This can be explained by the strong tendency of dipolar interactions to favor head-to-tail magnetic moment arrangements and flux closure (magnetic shape anisotropy). Furthermore, it is consistent with the already-mentioned reflection symmetry with respect to the lattice plane. The latter implies that the local dipolar fields acting on the magnetic moments $\vec{\mu}_k$ are always parallel to the xy plane when all the $\vec{\mu}_k$ are in-plane. Consequently, the energy increases quadratically whenever a $\vec{\mu}_k$ is rotated out of the xy plane [39,50,51]. In Fig. 1, one observes that the ground-state configurations, Figs. 1(a) and 1(b), are vortexlike with a vanishing, flux-closing magnetization in each hexagon. Consequently, the total magnetization of the nanostructure is also zero. If one decomposes the lattice into different hexagons, as sketched in Fig. 1(a), one observes that all hexagons have the same microvortex (MV) magnetic order. This magnetic configuration can be characterized by a single parameter η_{MV} , which defines the orientation of every magnetic moment $\vec{\mu}_k$ ($k = 1, \dots, 6$) in any given hexagon through the polar angle φ_k formed by $\vec{\mu}_k$ and the positive x axis. Explicitly, we have

$$\varphi_k = \left\{ -\eta_{MV} + \frac{2\pi}{3}, \eta_{MV} + \frac{2\pi}{3}, -\eta_{MV} - \frac{2\pi}{3}, \eta_{MV} - \frac{2\pi}{3}, -\eta_{MV}, \eta_{MV} \right\}, \quad (7)$$

for $k = 1, \dots, 6$, where η_{MV} is arbitrary ($\eta_{MV} \in [0, 2\pi]$) and the labeling of the NPs is anticlockwise starting from the NP located at the rightmost corner of each hexagon. Examples are shown in Fig. 1(a), which corresponds to $\eta_{MV} = 0$, and Fig. 1(b), which corresponds to $\eta_{MV} = \pi/6$. In a perfectly periodic lattice, the above-described ground-state MV configuration is continuously degenerate with respect to η_{MV} [29]. This is a consequence of the D_3 point-group symmetry at the lattice sites of the honeycomb lattice. The same type of symmetry-conditioned continuous degeneracy appears whenever the local symmetry group contains a C_n axis with $n > 2$, which renders the xy representation irreducible, as already observed in periodic square and triangular lattices [31,50]. The continuous degeneracy is removed by thermal fluctuations, structural disorder, and distortions, in which case specific values of η_{MV} are stabilized, an effect known as order-by-disorder [29,52,53]. For example, finite-temperature fluctuations break the continuous degeneracy of the lattice by stabilizing the angles $\eta_{MV} = n\pi/6$, with $n = 0, \dots, 5$ [29]. It is interesting to note that the thermally induced stabilization is much weaker in the honeycomb lattice than in the square lattice, where the angle between stabilized orientations ($\pi/2$) is larger. This is consistent with the idea that the barriers separating metastable states increase as their structural differences become more important (Hammond's postulate) [54].

In contrast to the ground state, the excited metastable states of the honeycomb lattice have finite degeneracies, which can be understood by taking into account the D_6 point-group symmetry with respect to the centers of the hexagons, the translational symmetries, and the time-reversal symmetry of the underlying Hamiltonian. The first-excited configuration, shown in Fig. 1(c), consists of vortices similar to the ground state combined with stripes of antiparallel arrangements of the magnetic moments. In this case the total magnetization vanishes as well. Since the translational symmetry of the magnetic order is partly reduced, one finds that 9 out of the 27 possible translations within the unit cell yield a different degenerate configuration [see Fig. 1(c)]. These translations together with the C_6 rotations of the D_6 group explain the 54fold degeneracy of the first metastable state. The other symmetry operations (reflections and time-reversal) do not yield any additional configurations.

The second-excited state illustrated in Fig. 1(d) also consists of flux-closing vortexlike arrangements of the magnetic moments. However, in contrast to the lower-lying states, the second-excited configuration presents no periodicity at all within the considered unit cell. Consequently, all 27 translations within the unit cell yield different degenerate configurations. Combined with the C_6 rotations of the D_6 group and with time-reversal symmetry, this raises the total degeneracy of the second metastable configuration to 324. The reflections of the D_6 group do not yield any new states. Overall, 13 qualitatively distinct metastable states have been found for the ensemble illustrated in Fig. 1 ($N = 54$). All of them have important degeneracies which can be explained by similar considerations. The largest degeneracy observed for the considered unit cell is 648. This occurs when all translations, rotations, and also reflections yield distinct magnetic configurations.

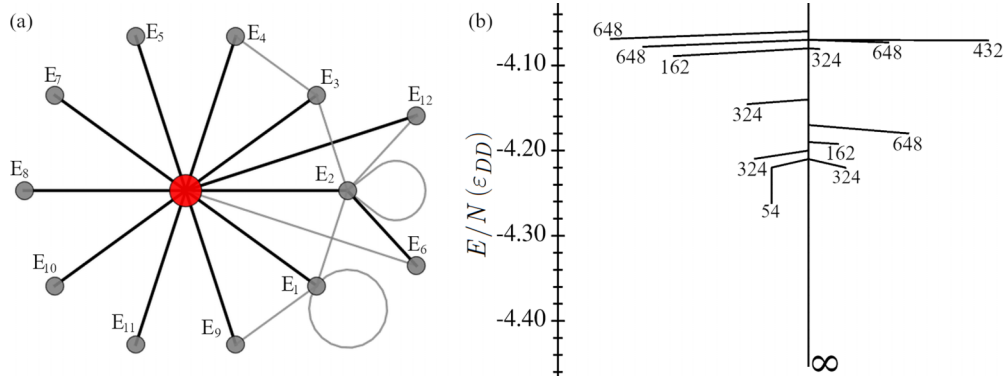


FIG. 2. (a) Kinetic network of a periodic honeycomb lattice with $N = 54$ dipole-coupled NPs in the unit cell. The degenerate ground state is represented by a red circle. The n th level of degenerate metastable states are grouped into the gray circles labeled E_n . The transitions towards the ground state are highlighted in black, whereas the transitions among the excited states are indicated in gray. (b) Corresponding disconnectivity graph, where the degenerate states are also grouped into a single branch and the degeneracies are given by the numbers at the end of each branch. Notice that the energies are measured in units of ε_{DD} [see Eq. (4)].

Previous studies have shown that ensembles of dipole-coupled magnetic moments have complex energy landscapes containing significant numbers of local minima and intermediate transition states [39,50,55]. For the honeycomb ensemble illustrated in Fig. 1, we find in total $N_{LM} = 4915$ local minima, if the continuously degenerate ground state is counted as one, and $N_{TS} = 22\,908$ transition states connecting them. A first insight into the topology of the energy landscape is provided by the kinetic network shown in Fig. 2(a). The nodes, which represent the LM, and the edges, which represent the TSs, display the connectivity among the LM. For the sake of clarity, degenerate LM have been grouped into a single node. Direct transitions between degenerate LM are sometimes possible as indicated by the gray loops in Fig. 2(a). One observes that the ground state is at the very center of the network (red node). It is a throughout-reaching hub, directly connected to all the excited metastable states and has a degree density $\rho = 1$. In contrast, the direct transitions among the excited metastable states are very few, with degree densities of the order of $\rho \approx 10^{-3}$. The resulting kinetic network is starlike with a very small transitivity $C \simeq 10^{-3}$ as there are only a small number of connections among some of the excited metastable states and therefore the KN is nearly bipartite. The starlike topology of the KN implies that the distance between any pair of metastable states is very small. In fact, each excited configuration is directly connected to the ground state ($d = 1$) and requires at most two elementary transitions ($d = 2$) to reach any other excited state. The resulting average path distance $\langle d \rangle = 1.99$ is thus extremely short.

From a physical perspective, the topology of the kinetic network of honeycomb ensembles is characteristic of systems where the relaxation dynamics is particularly fast and unhindered irrespectively of the initial configuration, since the ground state is at the center of the network and only one elementary transition is required to reach it from any metastable state. In addition, the relaxation towards the ground state is extremely funneled, as the connectivity among the excited states is very small. Thus, elementary transitions between pairs of excited states are relatively unlikely. One concludes that honeycomb NP arrangements are extremely good structure seekers. A comparable behavior has been found in periodic

square and triangular lattices, whose ground states are also continuously degenerate [39,50]. Furthermore, taking into account the results of Ref. [50], it is reasonable to expect that weakly disordered honeycomb nanostructures should behave in a similar way.

Kinetic networks certainly offer us a most useful insight on the connectivity among the metastable states of a system. However, they give no information on the energies of the metastable states and on the energy barriers separating them, which are also crucial for the dynamics. This important complementary perspective is provided by the disconnectivity graphs introduced in Sec. II C and shown in Fig. 2(b). To improve the readability of the DG, the degenerate LM are grouped in a single branch, with the corresponding degeneracy being indicated at the end of each branch. The continuously degenerate ground state can be easily identified at the bottom of the DG, clearly separated from the excited metastable states which all have significantly higher energies. Notice, that the downhill energy barriers from the excited states towards the ground state are comparatively small, typically at least 25 times smaller than the barriers in the opposite upward direction. The sole exception is the first-excited state for which the downhill barrier $\Delta E_{\downarrow} = 0.05 \varepsilon_{DD}$ is only around 5 times smaller than the uphill barrier $\Delta E_{\uparrow} = 0.24 \varepsilon_{DD}$. Therefore, the relaxation from any initial state will be rapid and irreversible, even at low temperatures, as in good structure seekers. The results confirm our analysis of the kinetic networks. They are in good agreement with the behavior found in other highly symmetric periodic lattices, such as the square and triangular lattices [39].

B. Kagome lattice

The kagome lattice is a triangular Bravais lattice defined by the primitive translation vectors

$$\vec{e}_1 = \lambda(2, 0) \quad \text{and} \quad \vec{e}_2 = \lambda(1, \sqrt{3}), \quad (8)$$

with a basis consisting of triangles with coordinates

$$\vec{e}_A = (0, 0) \quad \text{and} \quad \vec{e}_B = \lambda(1, 0), \quad \text{and} \quad \vec{e}_C = \frac{\lambda}{2}(1, \sqrt{3}), \quad (9)$$

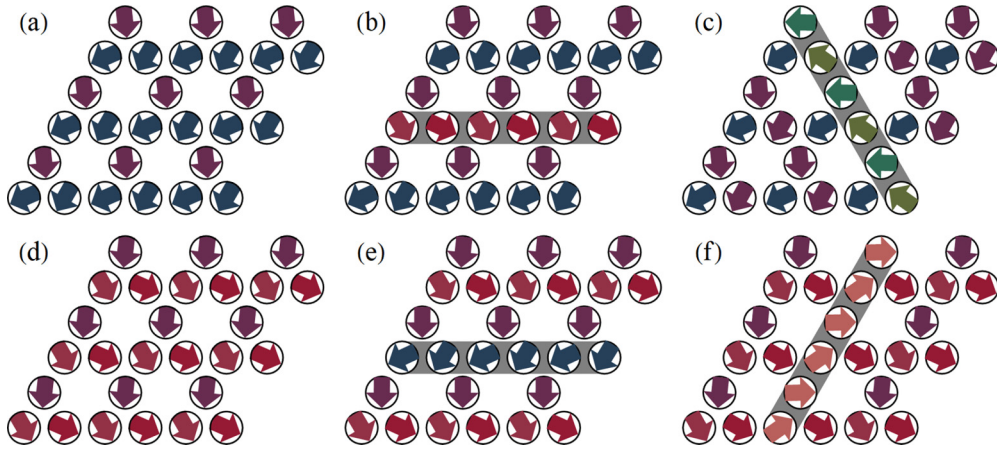


FIG. 3. Metastable magnetic configurations of a periodic kagome lattice with $N = 27$ dipole-coupled NPs in the unit cell. The circles indicate the position of the particles, while the arrows indicate the orientation of the magnetic moments within the xy plane. Examples of the 6-fold degenerate ground state are shown in panels (a) and (d). The other subfigures illustrate different degenerate magnetic configurations of the first-excited state, in which the changes with respect to the ground states are highlighted in gray.

where λ is the nearest-neighbor distance. In other words, the kagome lattice is a triangular lattice of triangles (see Fig. 3).

As already discussed in the previous section, all the magnetic moments in the relevant magnetic configurations, including LM, TSs, and MEPs, lie within the xy plane. This is a consequence of the nature of the dipolar interaction and the reflection symmetry of the NP arrangement across the lattice plane. Examples of the low-lying magnetic configurations of a kagome lattice having $N = 27$ NPs in the unit cell are illustrated in Fig. 3. Previous studies have shown that the ground state is 6-fold degenerate as a result of the C_3 rotational symmetry with respect to the centers of the triangles together with time-reversal symmetry [40,41]. The ground-state magnetic configurations reflect the translational symmetry of the underlying triangular Bravais lattice. Indeed the magnetic order is entirely defined by the orientation of $\vec{\mu}_k$ in one of the basis triangles. The magnetic moments in all the other triangles are oriented in the same way [see Figs. 3(a) and 3(d)]. This defines three sublattices, which we denote as A , B , and C , within which the magnetic moments are all parallel. In Table I, the polar angles φ_A , φ_B , and φ_C between $\vec{\mu}_k$ in the three sublattices and the x axis are given for all six degenerate ground states. One observes that the angles $\Delta\varphi = 0.64$ between the magnetic moments in each triangle are relatively small. Consequently, the ground-state magnetization is finite. Normalized per unit cell it amounts to $\mu = 0.87$.

TABLE I. The angles φ_A , φ_B , and φ_C defining the orientation of the magnetic moments at the sublattices A , B , and C of a kagome lattice with $N = 27$ NPs in the unit cell for the six degenerate ground-state configurations [40]. The configurations 1 and 4 are illustrated in Figs. 3(a) and 3(d), respectively.

	1	2	3	4	5	6
φ_A	3.55	0.41	3.78	0.64	2.09	5.24
φ_B	4.19	1.05	2.51	5.65	2.73	5.87
φ_C	4.82	1.68	π	0.00	1.46	4.60

From a local perspective, the kagome lattice can be regarded as an arrangement of horizontal and oblique chains of NPs, in which each NP is at the crossing of two chains (see Fig. 3). The magnetic order in the first-excited state, which is illustrated in Figs. 3(b), 3(c), 3(e), and 3(f), can be pictured in terms of these chains. One observes that the orientations of the magnetic moments in the first metastable configuration are, for the most part, very similar to the ones found in one of the ground states. The magnetic orders in Figs. 3(b) and 3(c) are very similar to those in Fig. 3(a), whereas the magnetic orders in Figs. 3(e) and 3(f) are similar to those in Fig. 3(d). The actual excitation consists of rotating the magnetic moments of a complete horizontal chain [Figs. 3(b) and 3(e)] or of an oblique chain [Figs. 3(c) and 3(f)]. The magnetic moments along these specific chains, which are highlighted in gray in Fig. 3, are rotated by $\Delta\varphi \simeq 1.62$ with respect to their ground-state orientation, such that the component of the magnetization along the chain is reversed. Furthermore, it is important to note that, starting from any ground-state configuration, only excitations along two of the three chain directions are observed. For instance, in the case of the ground state depicted in Fig. 3(a), only the excitations along the chain directions highlighted in Figs. 3(b) and 3(c) are possible. In fact, in order that the rotation of the moments along a chain yields a metastable configuration, the nearly head-to-tail arrangement of the magnetic moments needs to be preserved and the resulting angles φ_k of $\vec{\mu}_k$ in the triangles need to be close to those in one of the ground states (see Table I). Consequently, in the kagome lattice illustrated in Fig. 3, each ground state is connected to six different first-excited states, which corresponds to choosing one of the three different chains along the two directions. In larger unit cells with a greater number of NP chains, the ground states are connected to the corresponding larger number of excited states. Furthermore, it is most interesting to observe that, upon rotating the magnetic moments along the chains with respect to one ground state, some of the short-range correlations found in a different ground state are locally restored (i.e., showing a different set of φ_A , φ_B , and φ_C given in Table I). Compare, for instance, the

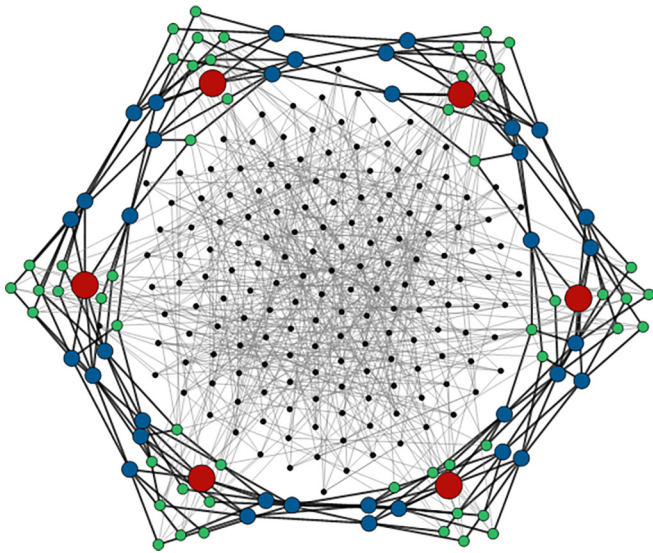


FIG. 4. Kinetic network of a periodic kagome lattice with $N = 27$ dipole-coupled NPs in the unit cell. The 6-fold degenerate ground states are highlighted by red dots, the first-excited states by blue dots, and the second-excited states by green dots. The local minima having higher energies are represented by the smaller black dots. The edges connecting the dots indicate the elementary transitions between the LM across first-order saddle points. Notice that the degree distribution among the nodes is very homogeneous and that the network lacks any hubs or centers through which relaxation could be funneled.

configurations shown in Figs. 3(a), 3(b), and 3(d) [40]. Thus, the first-excited states are always a mixture of two different ground states.

The metastable states with higher energies are obtained by rotating additional chains of magnetic moments along chains with different directions. Thus, short-range magnetic orders within the triangles are found which correspond to more than two different ground states. For instance, second-excited states can be obtained from the ground state shown in Fig. 3(a) by combining the first-excited states displayed in Figs. 3(b) and 3(c). Consequently, the second excitation is 54-fold degenerate, which amounts to the number of ground states times the number chains with proper orientations, in the present unit cell (6×9 , see Fig. 3). Higher-excited metastable states can be obtained in a similar way by successive moment rotations along different chains.

Figure 4 shows the kinetic network of the kagome lattice illustrated in Fig. 3. It consists of $N_{\text{LM}} = 258$ nodes representing the LM and $N_{\text{TS}} = 676$ edges representing elementary transitions between the LM across first-order saddle points. The 6-fold degenerate ground states are represented by red dots, the first-excited states are indicated by blue dots, and the second-excited states are indicated by green dots. The higher-energy excited states are indicated by black dots. Comparison with the honeycomb lattice [Fig. 2(a)] reveals remarkable differences. While in the honeycomb lattice the continuously degenerate ground-state was at the center of the KN, directly connected to all metastable states, in the kagome arrangement the degree distribution among all nodes is extremely homogeneous. In fact, with very few exceptions, each LM

is connected to exactly six other LM. This behavior can be explained by the nature of the excitations as discussed in previous paragraphs. For instance, if one considers the ground state shown in Fig. 3(a), excitations can only occur along the horizontal chains of NPs or along the oblique chains of NPs [see Figs. 3(b) and 3(c)]. Similar considerations explain the magnetic order in the other metastable states. In this context it is worth noting that no elementary transition has been found where the magnetic moments along more than one chain of NPs are rotated simultaneously. Changes in the magnetic order where the moments of more than one chain rotate are, of course, possible but they involve multiple elementary transitions.

In Fig. 4 one observes that the ground state and low-lying LM form a ring-like structure, which reflects the 6-fold degeneracy of the ground state. The higher-energy LM have been placed at the center of the KN shown in Fig. 4 merely for the sake of clarity. They do not constitute the center of the network from the perspective of network science. In fact, the kinetic network of the kagome lattice does not exhibit any center or hub through which the dynamics could be funneled, as it is the case in the honeycomb lattice. In the context of network science one refers to this type of network as being latticelike, since the degree of all nodes is small and nearly the same. This implies that the distance between nodes can be very large [56,57]. Indeed, one may furthermore note that the average path distance $\langle d \rangle = 4.4$ is comparatively large and that the KN is bipartite ($C = 0$). In summary, kagome systems are very much the opposite of good structure seekers, in strong contrast to the honeycomb, square, or triangular ensembles, for example (see Sec. III A and Refs. [39,50]).

The DG of the kagome NP lattice is shown in Fig. 5. One observes that the energies of the 6-fold degenerate ground state ($E_0 = -4.778 \varepsilon_{DD}$) and of the 36-fold degenerate first-excited metastable state ($E_1 = -4.774 \varepsilon_{DD}$) are extremely close yet the magnetic orders in these states are distinct, as previously discussed. Notice, moreover, that all these magnetic configurations are remarkably stable locally. They are separated from the adjacent metastable states by comparatively large energy barriers: $\Delta E_0 = 0.154 \varepsilon_{DD}$ and $\Delta E_1 = 0.135 \varepsilon_{DD}$. The 54-fold degenerate second-excited states lie at an appreciably higher energy $E_2 = -4.706 \varepsilon_{DD}$, while the remaining LM have much higher energies $E_3 = -4.636 \varepsilon_{DD}$ and $E_4 = -4.635 \varepsilon_{DD}$. The energy profiles are, in general, quite asymmetric, as in the honeycomb lattice. However, notice that the downhill barriers are much larger than those in the honeycomb ensemble, although they are still small in comparison to the much bigger uphill barriers.

Qualitatively, the DG of the kagome ensemble shown in Fig. 5 can be divided into two parts. The upper part including the states with the higher energies E_3 and E_4 resembles a palm tree as found, for instance, in the honeycomb lattice. Consequently, the relaxation out of these states is expected to be unhindered and fast towards the low-energy states, even at relatively low temperatures. In contrast, the lower part of the DG shows no hierarchy among the LM. Instead, one finds a large number of LM having extremely close energies and large energy barriers separating them. In addition, the analysis of the KN has shown that the distances in configurational space between these low-energy LM are large, as given

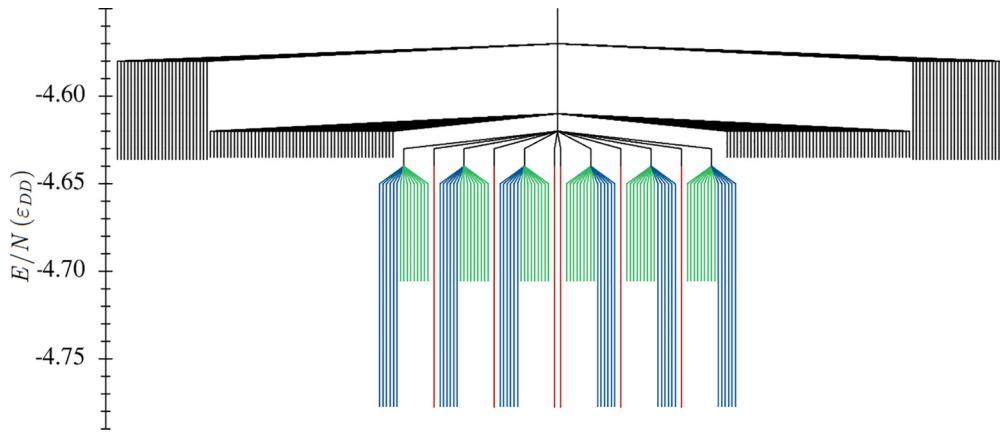


FIG. 5. Disconnectivity graph of the energy landscape of a periodic kagome lattice with $N = 27$ dipole-coupled NPs in the unit cell, which contains $N_{\text{LM}} = 298$ local minima. The colors indicate the ground states (red), first-excited states (blue), second-excited states (green), and higher-energy LM (black), as in Fig. 4. The energies on the y axis are given in units of ϵ_{DD} [see Eq. (1)].

by the important number of elementary transitions between them. Therefore, one expects a very slow relaxation dynamics involving trapping and an extremely difficult approach to equilibrium.

Calculations on larger systems have also been performed in order to assess how the results are affected by the unit-cell size and the periodic boundary conditions. The thus obtained magnetic configurations are extremely similar to those previously described in this work. This applies in particular to the ground state, whose 6-fold degeneracy does not change. However, the number of low-lying LM increases most rapidly as the number of NPs in the unit cell is increased. For instance, in the case of $N = 48$ NPs, we find a 48-fold degenerate first-excited state, a 36-fold degenerate second-excited state, and a 36-fold degenerate third excited state, whose energies are all extremely close to the ground-state energy and which are all separated from each other by important energy barriers. This confirms and in fact strengthens the validity of the analysis presented in previous paragraphs. Concerning the energy barriers between the LM, one observes that their height ΔE increases, as expected, as a function of N , while the ratio $\Delta E/N$ tends to decrease. In sum, the calculations show that considering larger unit cells does not affect our conclusions in a qualitative way.

IV. CONCLUSION

The energy landscapes of dipole-coupled magnetic nanoparticles organized in two-dimensional periodic honeycomb and kagome lattices have been investigated. The corresponding ergodic networks of local minima and connecting transition states have been determined and analyzed in some detail. Remarkable specific properties as well as strong qualitative differences in the physical behavior of these systems have been revealed. Honeycomb lattices are shown to be very good structure seekers. In this case one observes that almost any metastable magnetic configuration can evolve into the continuously degenerate ground state by overcoming a relatively small energy barrier through a single first-order transition state. The kinetic networks of these nanostructures are starlike and the disconnectivity graphs resemble palm trees. One concludes that the magnetic behavior of

honeycomb lattices of magnetic NPs are qualitatively very close to that observed for periodic square and triangular lattices [39]. In contrast, kagome lattices of magnetic NPs show a large number of low-energy metastable states, which have very similar energies and are separated by large energy barriers. The corresponding kinetic networks of stationary points resemble periodic lattices, where all the nodes representing the LM have a very similar small number of direct links to other nodes, the average path distance between nodes is large, and no hubs or hierarchy among the nodes can be identified. The disconnectivity graphs show that the relaxation from high-energy configurations towards the low-energy part of the EL should be relatively fast. However, the large multiplicity of metastable states with very similar low energies and the presence of large energy barriers separating them should result in trapping and in an extremely slow relaxation towards equilibrium.

The main purpose of this paper has been to characterize the collective magnetic behavior of dipole-coupled magnetic nanoparticles organized in specific two-dimensional periodic structures. It would be very interesting to extend the present investigations by taking into account a number of additional magnetic effects. For example, one could incorporate local energy contributions, such as shape-induced and magnetocrystalline anisotropies of individual nanoparticles, as well as the coupling to external magnetic fields, in order to quantify how they compete with the dipolar interactions. This is expected to result in significant changes in the collective magnetic response of the different NP arrangements. Further developments include a more detailed description of the magnetostatic interactions through higher-order multipole contributions, which should be significant when the shape of the nano-objects is far from spherical. Finally, the study of other forms of interparticle interactions, for instance, those mediated by a metallic support, represent a further challenging research direction.

ACKNOWLEDGMENT

Computer resources provided by the IT Service Center of the University of Kassel are gratefully acknowledged.

- [1] C. Nisoli, R. Moessner, and P. Schiffer, Colloquium: Artificial spin ice: Designing and imaging magnetic frustration, *Rev. Mod. Phys.* **85**, 1473 (2013).
- [2] A. Farhan, P. M. Derlet, A. Kleibert, A. Balan, R. V. Chopdekar, M. Wyss, J. Perron, A. Scholl, F. Nolting, and L. J. Heyderman, Direct observation of thermal relaxation in artificial spin ice, *Phys. Rev. Lett.* **111**, 057204 (2013).
- [3] L. Anghinolfi, H. Luetkens, J. Perron, M. G. Flokstra, O. Sendetskiy, A. Suter, T. Prokscha, P. M. Derlet, S. Lee, and L. J. Heyderman, Thermodynamic phase transitions in a frustrated magnetic metamaterial, *Nat. Commun.* **6**, 8278 (2015).
- [4] E. Östman, H. Stopfel, I.-A. Chioar, U. B. Arnalds, A. Stein, V. Kapaklis, and B. Hjörvarsson, Interaction modifiers in artificial spin ices, *Nat. Phys.* **14**, 375 (2018).
- [5] R. Streubel, N. Kent, S. Dhuey, A. Scholl, S. D. Kevan, and P. Fischer, Spatial and temporal correlations of XY macro spins, *Nano Lett.* **18**, 7428 (2018).
- [6] N. A. Frey and S. Sun, Magnetic nanoparticle for information storage applications, in *Inorganic Nanoparticles: Synthesis, Applications, and Perspectives*, edited by C. Altavilla and E. Ciliberto (CRC, Boca Raton, 2010), Chap. 2, pp. 33–68.
- [7] S. Karmakar, S. Kumar, R. Rinaldi, and G. Maruccio, Nano-electronics and spintronics with nanoparticles, *J. Phys.: Conf. Ser.* **292**, 012002 (2011).
- [8] B. Dieny, I. L. Prejbeanu, K. Garello, P. Gambardella, P. Freitas, R. Lehdorff, W. Raberg, U. Ebels, S. O. Demokritov, J. Akerman, A. Deac, P. Pirro, C. Adelmann, A. Anane, A. V. Chumak, A. Hirohata, S. Mangin, S. O. Valenzuela, M. C. Onbaşlı, M. d'Aquino *et al.*, Opportunities and challenges for spintronics in the microelectronics industry, *Nat. Electron.* **3**, 446 (2020).
- [9] S. D. Sloetjes, E. S. Digernes, A. Stromberg, F. K. Olsen, A. D. Bang, A. T. N'Diaye, R. V. Chopdekar, E. Folven, and J. K. Grepstad, Effects of array shape and disk ellipticity in dipolar-coupled magnetic metamaterials, *Phys. Rev. B* **104**, 134421 (2021).
- [10] K. Lee, J. Callaway, and S. Dhar, Electronic structure of small iron clusters, *Phys. Rev. B* **30**, 1724 (1984).
- [11] K. Lee, J. Callaway, K. Kwong, R. Tang, and A. Ziegler, Electronic structure of small clusters of nickel and iron, *Phys. Rev. B* **31**, 1796 (1985).
- [12] I. M. L. Billas, J. A. Becker, A. Chatelain, and W. A. de Heer, Magnetic moments of iron clusters with 25 to 700 atoms and their dependence on temperature, *Phys. Rev. Lett.* **71**, 4067 (1993).
- [13] J. P. Bucher, D. C. Douglass, and L. A. Bloomfield, Magnetic properties of free cobalt clusters, *Phys. Rev. Lett.* **66**, 3052 (1991).
- [14] R. A. Guirado-López, J. Dorantes-Dávila, and G. M. Pastor, Orbital magnetism in transition-metal clusters: From Hund's rules to bulk quenching, *Phys. Rev. Lett.* **90**, 226402 (2003).
- [15] G. M. Pastor, J. Dorantes-Dávila, and K. H. Bennemann, Size and structural dependence of the magnetic properties of small 3d-transition-metal clusters, *Phys. Rev. B* **40**, 7642 (1989).
- [16] G. M. Pastor, J. Dorantes-Dávila, S. Pick, and H. Dreyse, Magnetic anisotropy of 3d transition-metal clusters, *Phys. Rev. Lett.* **75**, 326 (1995).
- [17] M. Muñoz-Navia, J. Dorantes-Dávila, D. Zitoun, C. Amiens, N. Jaouen, A. Rogalev, M. Respaud, and G. M. Pastor, Tailoring the magnetic anisotropy in CoRh nanoalloys, *Appl. Phys. Lett.* **95**, 233107 (2009).
- [18] D. C. Douglass, A. J. Cox, J. P. Bucher, and L. A. Bloomfield, Magnetic properties of free cobalt and gadolinium clusters, *Phys. Rev. B* **47**, 12874 (1993).
- [19] W. A. de Heer, P. Milani, and A. Chatelain, Spin relaxation in small free iron clusters, *Phys. Rev. Lett.* **65**, 488 (1990).
- [20] D. Schildknecht, L. J. Heyderman, and P. M. Derlet, Phase diagram of dipolar-coupled XY moments on disordered square lattices, *Phys. Rev. B* **98**, 064420 (2018).
- [21] S. K. Baek, P. Minnhagen, and B. J. Kim, Kosterlitz-Thouless transition of magnetic dipoles on the two-dimensional plane, *Phys. Rev. B* **83**, 184409 (2011).
- [22] B. Alkadour, J. I. Mercer, J. P. Whitehead, B. W. Southern, and J. van Lierop, Dipolar ferromagnetism in three-dimensional superlattices of nanoparticles, *Phys. Rev. B* **95**, 214407 (2017).
- [23] M. Varón, M. Beleggia, T. Kasama, R. J. Harrison, R. E. Dunin-Borkowski, V. F. Puentes, and C. Frandsen, Dipolar magnetism in ordered and disordered low-dimensional nanoparticle assemblies, *Sci. Rep.* **3**, 1234 (2013).
- [24] P. Torche, C. Munoz-Menendez, D. Serantes, D. Baldomir, K. L. Livesey, O. Chubykalo-Fesenko, S. Ruta, R. Chantrell, and O. Hovorka, Thermodynamics of interacting magnetic nanoparticles, *Phys. Rev. B* **101**, 224429 (2020).
- [25] E. H. Sánchez, M. Vasilakaki, S. S. Lee, P. S. Normile, M. S. Andersson, R. Mathieu, A. López-Ortega, B. P. Pichon, D. Peddis, C. Binns, P. Nordblad, K. Trohidou, J. Nogués, and J. A. D. Toro, Crossover from individual to collective magnetism in dense nanoparticle systems: Local anisotropy versus dipolar interactions, *Small* **18**, 2106762 (2022).
- [26] P. J. Jensen and G. M. Pastor, Dipole coupling induced magnetic ordering in an ensemble of nanostructured islands, *Phys. Status Solidi A* **189**, 527 (2002).
- [27] P. J. Jensen and G. M. Pastor, Low-energy properties of two-dimensional magnetic nanostructures: Interparticle interactions and disorder effects, *New J. Phys.* **5**, 68 (2003).
- [28] G. M. Pastor and P. J. Jensen, Elementary transitions and magnetic correlations in two-dimensional disordered nanoparticle ensemble, *Phys. Rev. B* **78**, 134419 (2008).
- [29] S. Prakash and C. L. Henley, Ordering due to disorder in dipolar magnets on two-dimensional lattices, *Phys. Rev. B* **42**, 6574 (1990).
- [30] P. Politi, M. G. Pini, and R. L. Stamps, Dipolar ground state of planar spins on triangular lattices, *Phys. Rev. B* **73**, 020405(R) (2006).
- [31] D. Schildknecht, M. Schütt, L. J. Heyderman, and P. M. Derlet, Continuous ground-state degeneracy of classical dipoles on regular lattices, *Phys. Rev. B* **100**, 014426 (2019).
- [32] B. E. Skovdal, G. K. Palsson, P. C. W. Holdsworth, and B. Hjörvarsson, Emergent tricriticality in magnetic metamaterials, *Phys. Rev. B* **107**, 184409 (2023).
- [33] D. Mehta, C. Hughes, M. Schröck, and D. J. Wales, Potential energy landscapes for the 2D XY model: Minima, transition states and pathways, *J. Chem. Phys.* **139**, 194503 (2013).
- [34] D. Mehta, C. Hughes, M. Kastner, and D. J. Wales, Potential energy landscapes of the two-dimensional XY model: Higher-index stationary points, *J. Chem. Phys.* **140**, 224503 (2014).
- [35] T. Jonsson, J. Mattsson, C. Djurberg, F. A. Khan, P. Nordblad, and P. Svedlindh, Aging in a magnetic particle system, *Phys. Rev. Lett.* **75**, 4138 (1995).

- [36] M. Sasaki, P. E. Jönsson, H. Takayama, and H. Mamiya, Aging and memory effects in superparamagnets and superspin glasses, *Phys. Rev. B* **71**, 104405 (2005).
- [37] D. Parker, V. Dupuis, F. Ladieu, J.-P. Bouchaud, E. Dubois, R. Perzynski, and E. Vincent, Spin-glass behavior in an interacting γ -Fe₂O₃ nanoparticle system, *Phys. Rev. B* **77**, 104428 (2008).
- [38] M. Vasilakaki, G. Margaritis, D. Peddis, R. Mathieu, N. Yaacoub, D. Fiorani, and K. Trohidou, Monte Carlo study of the superspin glass behavior of interacting ultrasmall ferrimagnetic nanoparticles, *Phys. Rev. B* **97**, 094413 (2018).
- [39] D. Gallina and G. M. Pastor, Theory of the collective behavior of two-dimensional periodic ensembles of dipole-coupled magnetic nanoparticles, *Phys. Rev. B* **107**, 184407 (2023).
- [40] M. S. Holden, M. L. Plumer, I. Saika-Voivod, and B. W. Southern, Monte Carlo simulations of a kagome lattice with magnetic dipolar interactions, *Phys. Rev. B* **91**, 224425 (2015).
- [41] M. Maksymenko, V. R. Chandra, and R. Moessner, Classical dipoles on the kagome lattice, *Phys. Rev. B* **91**, 184407 (2015).
- [42] O. Benton, Ordered ground states of kagome magnets with generic exchange anisotropy, *Phys. Rev. B* **103**, 174425 (2021).
- [43] D. J. Wales, *Energy Landscapes: Applications to Clusters, Biomolecules and Glasses* (Cambridge University, Cambridge, England, 2004).
- [44] J. P. K. Doye and D. J. Wales, The effect of the range of the potential on the structure and stability of simple liquids: From clusters to bulk, from sodium to C₆₀, *J. Phys. B* **29**, 4859 (1996).
- [45] M. A. Miller, J. P. K. Doye, and D. J. Wales, Structural relaxation in Morse clusters: Energy landscapes, *J. Chem. Phys.* **110**, 328 (1999).
- [46] J. Nocedal, Updating quasi-Newton matrices with limited storage, *Math. Comp.* **35**, 773 (1980).
- [47] J. C. Mauro, R. J. Loucks, and J. Balakrishnan, A simplified eigenvector-following technique for locating transition points in an energy landscape, *J. Phys. Chem. A* **109**, 9578 (2005).
- [48] R. D. Luce and A. D. Perry, A method of matrix analysis of group structure, *Psychometrika* **14**, 95 (1949).
- [49] O. M. Becker and M. Karplus, The topology of multidimensional potential energy surfaces: Theory and application to peptide structure and kinetics, *J. Chem. Phys.* **106**, 1495 (1997).
- [50] D. Gallina and G. M. Pastor, Disorder-induced transformation of the energy landscapes and magnetization dynamics in two-dimensional ensembles of dipole-coupled magnetic nanoparticles, *Phys. Rev. X* **10**, 021068 (2020).
- [51] Besides the planar magnetic configurations with in-plane $\vec{\mu}_k$, which yield the low-energy magnetic configurations for dipolar interactions and thus represent the physically most relevant part of the EL, attention should, in principle, be paid to the perpendicular configurations, in which all the $\vec{\mu}_k$ are normal to the xy plane, because in these cases the dipolar fields at the lattice sites are also perpendicular to the lattice plane. Consequently, all perpendicular configurations are stationary points of the EL. We have, therefore, explicitly analyzed the nature of these stationary points by diagonalizing the Hessian matrix for a number of representative configurations including ferromagnetic (FM) and antiferromagnetic (AFM) perpendicular orders. The results show that these configurations are higher-order saddle points with relatively high energies. For instance, the FM perpendicular configuration of the honeycomb lattice is a 75th-order saddle point whose energy is $\Delta E = 11.04 \varepsilon_{DD}$ above the ground state. Moreover, the AFM perpendicular configuration is a 35th-order saddle point with $\Delta E = 2.12 \varepsilon_{DD}$. These values should be compared with the barrier energies between in-plane configurations, which are of the order of $0.1 \varepsilon_{DD}$.
- [52] J. Villain, R. Bidaux, J.-P. Carton, and R. Conte, Order as an effect of disorder, *J. Phys. Fr.* **41**, 1263 (1980).
- [53] C. L. Henley, Ordering due to disorder in a frustrated vector antiferromagnet, *Phys. Rev. Lett.* **62**, 2056 (1989).
- [54] G. S. Hammond, A correlation of reaction rates, *J. Am. Chem. Soc.* **77**, 334 (1955).
- [55] D. Gallina and G. M. Pastor, Structural disorder and collective behavior of two-dimensional magnetic nanostructures, *Nanomaterials* **11**, 1392 (2021).
- [56] A. L. Barabási, *Network Science* (Cambridge University, Cambridge, England, 2016).
- [57] M. E. J. Newman, *Networks* (Oxford University, Oxford, 2010).